CBPF-NF-064/96

Damage Spreading in a $2D$ Potts Ferromagnet in an External Field

L. da Silva[†], *F.A. Tamarit*[‡] *and A.C.N. de Magalhães*[†] *

[†]Centro Brasileiro de Pesquisas Físicas - CBPF
Rua Dr. Xavier Sigaud, 150
22290-180 Rio de Janeiro, RJ, Brazil

[‡] Fa.M.A.F., Universidad Nacional de Córdoba
Ciudad Universitaria, 5000 Córdoba, Argentina

October, 1996

Abstract

We study, through the damage spreading method and within the heat bath dynamics, the dynamical behavior of the square lattice 3-state Potts ferromagnet subjected to an external field. In the zero field case, we verify that this very simple model presents, besides the transition consistent with the equilibrium one, a new dynamical chaotic phase with unusual features. Although the unexpected transition occurs, within the error bars, at the static Ising critical temperature, it is in the directed percolation universality class. We observe that the application of an uniform magnetic field does not destroy any of the two transitions, while the unexpected one is annihilated by a new kind of field which plays the role of a conjugate field to the Hamming distance.

Key-words: Damage spreading; Potts model; Dynamical phase transitions; Heat bath dynamics

*__E-mails:__ ladario@cat.cbpf.br, tamarit@fis.uncor.edu and aglae@cat.cbpf.br

I. INTRODUCTION

The damage spreading technique [1,22] has been largely employed in the study of time-dependent critical phenomena in spin systems. In this method one essentially monitors the time evolution of two or more copies of the same system with different initial configurations subjected to a specific dynamics and to the *same* thermal noise. The usual monitored quantity is the Hamming distance or *damage* $D(t)$ defined as the fraction of elements which differ between the two configurations. The variation of the damage and related quantities with time, temperature, initial conditions and any other relevant parameter leads to information about the criticality of the system.

The results from damage spreading process can be quite different for distinct dynamics (see, for example [20]). For instance, in the Ising ferromagnet the spreading transition seems to coincide with the static critical temperature [2–4,17] if one uses the heat bath dynamics, while the opposite happens within the Glauber stochastic process [7,18].

In more complex systems, like the $2D$ anisotropic next-nearest neighbor Ising (ANNNI) model [3], the $3D$ and mean field spin glasses [2,10,16], the $2D$ XY ferromagnet [5], the $3D$ Heisenberg model [13], the p-state ($5 \leq p \leq 10$) clock model [12] and a soluble dilute ferromagnetic model [11], it has been found more than two dynamical phases where a few of them have no clearly known static equivalent. In the $3D$ spin glasses within the heat bath dynamics [2,10] and $2D$ XY ferromagnet within the Metropolis dynamics [5], it was obtained 3 different regimes where the lower transition temperature seems to agree with the equilibrium one, and it corresponds to the temperature above which the damage looses its dependence on the initial damage. The upper transition temperature (above which the damage vanishes) is consistent, in the case of spin glasses, with the temperature below which stretched exponential relaxations start to appear [23,24].

All the systems with three or more dynamical phases studied so far have some complex features, like competing interactions, dilution, continuous symmetry, non-trivial discrete symmetry (Z_q for $q \geq 5$), etc. One, then, may pose the question if this would be possible in a system without such degree of complexity. We verify herein, through the damage spreading technique, that *a very simple model*, namely the square lattice 3-state Potts ferromagnet subjected to the usual heat bath dynamics, has a *three-phase structure*. Its

corresponding static model has been extensively studied (for a review on the q-state Potts model see [25]) and, in particular, it has a continuous para-ferromagnetic phase transition at the exact critical temperature $k_B T_c\ (q=3)/J = [\ln(1+\sqrt{3})]^{-1}$ with precisely determined critical exponents. Concerning its dynamics, much less is known about it. In particular, a lot of emphasis has been given to the determination of the dynamic critical exponent z calculated at the dynamical transition which occurs at the mentioned equilibrium T_c. The region above T_c has not, in our knowledge, been explored such that one could guarantee that there is no change of regime in this region. Notice also that the investigation of the dynamical behavior of the Potts model through the damage spreading technique has not been published.†

Another interesting point which has hardly been investigated is the identification of the conjugate field associated with continuous dynamical transitions. It has been found [7,18] in the $2D$ and $3D$ Ising ferromagnet subjected to the Glauber dynamics, that an external uniform magnetic field B does not destroy the damage transition. Recently, two of us [15] have verified that a new kind of external field h, introduced in the literature [28] in the context of cellular automata (see also [29] for a mean-field version of it), plays the role of a conjugate field to the Hamming distance in the case of the Ising ferromagnet subjected to the heat-bath stochastic process. This field is defined as the frequency at which different random numbers are used for updating the two replicas. We also study, in this paper, the influences of both external fields B and h on the dynamical transitions of the $2D$ 3-state Potts ferromagnet.

The outline of this paper is the following. In section 2 we describe the above model and the spreading of damage method which we use. In section 3 we present our results in a zero field, while in section 4 we study the influence of external fields on the dynamical phase diagram. Finally, the conclusions are given in section 5. Notice that a short account of part of the zero field results has already been reported [30].

---

†We have learned of two related works in progress [26,27], one of them [26] studying the appearance of first order dynamical transitions for higher values of the number of states q.

II. MODEL AND METHOD

Let us associate with each site i of the square lattice a Potts variable σ_i which can assume $q = 3$ integer values ($\sigma_i = 0, 1$ and 2) and consider the Potts ferromagnet model described by the following Hamiltonian:

$$H = -J \sum_{(ij)} \delta(\sigma_i, \sigma_j) - B \sum_i \delta(\sigma_i, 0), \qquad (\sigma_i = 0, 1, 2, \cdots, q-1), \tag{1}$$

where $J > 0$ is the ferromagnetic coupling constant between nearest-neighbor spins, B is an external homogeneous magnetic field applied to the state $\sigma_i = 0$, and $\delta(\sigma_i, \sigma_j)$ is the Kronecker delta function. The first sum is over all the nearest-neighbor spins $< ij >$, while the second one is over all sites i of the square lattice.

Later on, instead of a magnetic field, we shall apply the above mentioned external field h in order to check if it destroys any of the transitions at $h = 0$ and if it leads to the divergence of its associated susceptibility at its transition temperature.

Our numerical simulations are implemented on squares with N spins and linear size $L (N = L^2$ sites) submitted to periodic boundary conditions. For updating the spin variables we use a sequential Monte Carlo heat-bath process (in a fully vectorized code). At each Monte Carlo step (MCS) t and for a given spin $\sigma_i(t)$ at site i, we compute first the energy differences $\Delta E_i^{\alpha\beta}(t) = E_i^{\beta} - E_i^{\alpha}$ for changing the spin $\sigma_i(t)$ at the state α into the state $\beta (\alpha, \beta = 0, 1, 2)$, and afterwards calculate the probabilities $p_i^{(\alpha)}$ ($\alpha = 0, 1, 2$) for $\sigma_i(t+1)$ to be in the state α, namely:

$$p_i^{(0)} = [1 + exp\ (-\beta \Delta E_i^{(01)}) + exp\ (-\beta \Delta E_i^{(02)})]^{-1}, \tag{2}$$

$$p_i^{(1)} = [1 + exp\ (\beta \Delta E_i^{(01)}) + exp\ (-\beta \Delta E_i^{(12)})]^{-1}, \tag{3}$$

$$p_i^{(2)} = [1 + exp\ (\beta \Delta E_i^{(02)}) + exp\ (\beta \Delta E_i^{(12)})]^{-1} = 1 - p_i^{(0)} - p_i^{(1)}, \tag{4}$$

where $\beta = 1/k_B T$ and T is the temperature of the system. The new state $\sigma_i(t+1)$ of the spin σ_i is then determined by comparing a chosen pseudo-random number $r_i(t) \in [0, 1]$ with the above probabilities according to the following rule:

$$\sigma_i(t+1) = \begin{cases} 0 \ \text{if} \ r_i(t) \leq p_i^{(0)} \\ 1 \ \text{if} \ p_i^{(0)} < r_i(t) \leq p_i^{(0)} + p_i^{(1)} \\ 2 \ \text{if} \ p_i^{(0)} + p_i^{(1)} < r_i(t) \leq 1 \end{cases} \tag{5}$$

Let us consider two different initial configurations $\{\sigma_i^{(A)}(0)$ and $\{\sigma_i^B(0)\}$ at time $t = 0$ and let them evolve according to the above dynamics submitted to the *same* thermal noise, i.e., using the same sequence of random numbers for updating the spins. We shall compare the two configurations $\{\sigma_i^A(t)\}$ and $\{\sigma_i^B(t)\}$ through the following distance $D(t)$ between them:

$$D(t) = \frac{1}{N}\sum_{i=1}^{N}[1 - \delta(\sigma_i^A(t), \sigma_i^B(t))], \tag{6}$$

where the sum is over all the N sites. Defined in this way, $D(t)$ is the fraction of spins which differ in the two replicas at time t.

In order to average $D(t)$ over thermal fluctuations we repeat the simulations for M samples, which leads to the average damage $< D(t) >$:

$$< D(t) >= \lim_{M\to\infty} \frac{\sum_{s=1}^{M} D_s(t)}{M}, \tag{7}$$

where $D_s(t)$ is the distance measured at time t for the $s-th$ sample.

If two configurations become identical at time t they will remain identical for all later times since they are updated with the same sequence of random numbers. Consequently we can introduce the *survival probability* $P(t)$ of two configurations being still different at time t given by

$$P(t) = \lim_{M\to\infty} \frac{M_1(t)}{M}, \tag{8}$$

where $M_1(t)$ is the number of samples such that $\{\sigma_i^A(t)\}$ and $\{\sigma_i^B(t)\}$ are still different at time t. Therefore, we can rewrite (7) as:

$$< D(t) >=< d(t) > P(t), \tag{9}$$

where $< d >$ is measured over only those $M_1(t)$ samples which have survived.

Throughout this paper we consider mainly three different sets of initial configurations for the two replicas, namely

(a) ordered along distinct states: $\{\sigma_i^A(0) = 0, \forall_i\}$ and $\{\sigma_i^B(0) = 1,\ \forall_i\}$ $(D(0) = 1)$;

(b) configuration $\{\sigma_i^A(0)\}$ is random and configuration $\{\sigma_i^B(0)\} = \{\sigma_i^A(0)\}$ except for 50% of the spins which are randomly chosen and given any of the two other possible states with equiprobability $(D(0) = 1/2)$;

(c) same as in (b) except for 5% of the chosen spins that are different ($D(0) = 0.05$).

As we will see in the next section, in some situations we need to compare the evolution of *three* distinct replicas A, B and C. In this case, we use the following set of initial configurations:

(d) same as in (b) and configuration $\{\sigma_i^C(0) \neq \sigma_i^A(0)\ \forall_i\}$ where to each spin of replica C is given any of the two other possible states with equiprobability ($D_{AB}(0) = 1/2$ and $D_{AC}(0) = 1$).

III. ZERO FIELD RESULTS

A. DYNAMICAL PHASE DIAGRAM

We show in Fig. 1 the survival probability $P(t)$ as a function of temperature T for the set of initial configurations (c) at different times t examining samples of linear size $L = 64$. First of all, notice that, at $t = 10000$, $P(t)$ has already achieved a stationary value for this size. Concerning its temperature dependence, we clearly observe *three* distinct regimes: i) a low-temperature one (for $T < T_2$, with $T_2 \simeq 1.0$) where P varies in a non abrupt way with T; ii) an intermediate regime (for $T_2 \leq T < T_1$, with $T_1 \simeq 1.2$) where $P = 1$ for all T; iii) a high-temperature one (for $T \geq T_1$) where $P = 0$. Similar behaviors (not presented herein) are obtained for other sizes ($L = 16$ and 32) and for the set of initial configurations (b). The abrupt variations of P near T_1 and T_2 indicate the existence of dynamical transitions at these temperatures. Leroyer and Rouidi [12] observed a similar behavior, starting from $D(0) = 1$, in the two higher transition temperatures (see their Fig. 9) of the p-state clock model ($5 \leq p \leq 10$). This is in contrast with the behavior found for the $3D$ Ising ferromagnet [2] where P, for any fixed $D(0)$, decreases slowly with an increasing T until it vanishes at the critical temperature.

In Figures 2 we exhibit the temporal behaviors of $P(t)$, $< d(t) >$ and $< D(t) >$ for fixed temperatures using the set of initial configurations (b). For a temperature $T = 0.90 < T_2$, we see from Fig. 2a that all these 3 quantities stay more or less stationary during the first MCS (roughly around 500 MCS) and afterwards vary during a transient time interval Δt_0

until they fluctuate around non-zero stationary values. We observed similar behaviors (not presented herein) for other values of $T < T_2$ and, as the temperature increases towards the transition temperature T_2, the time Δt_0 becomes longer and longer. For comparison, we also present in Fig. 2a $< d(t) >$ (by a full line) for the set of initial configurations (a): this line coincides with $< D(t) >$ since, for $D(0) = 1$, $P(t)$ equals 1. Notice that $< d(t) >$ for both sets of initial conditions (a) and (b) seem to converge to the same long-time limit, while this fact does not happen with the damage $< D(t) >$. Therefore, $< d(t) >$ is not a convenient distance for studying the evolution of the two replicas for $T < T_2$ since, if one waits for a sufficient long but finite time, one will not see the low-temperature regime (i). In other words, in this situation T_2 would tend to zero as it happened in the Ising ferromagnet [2] whose temperature behavior of $P(t)$ has only *two*, instead of three regimes.

For $T = 1.06$, one can see from Fig. 2b that the transient interval Δt_0 is very small (Δt_0 is roughly $100 MCS$) and $P(t)$ equals 1, leading thus to the equality $< d(t) >=< D(t) >$. As we change the temperature in this intermediate regime ($T_2 \leq T < T_1$), we obtain (not shown herein) a similar behavior, with Δt_0 increasing as we approach T_1. In this whole temperature regime the simulations remain unaltered if we use other sets of initial configurations, showing that both $< D(t) >$ and $< d(t) >$ become independent of $D(0)$ and that $P(t) = 1$ in this region.

In the high-temperature regime (iii) (for $T \geq T_1$), our simulations (not shown herein) show that $P(t)$, $< d(t) >$ and $< D(t) >$ fall off to zero after a transient time interval Δt_0, which decreases rapidly to zero as we increase the temperature difference between T and T_1.

For the reasons given above, we will henceforth focus our attention exclusively into quantities which are averaged over *all* M samples, rather than over the M_1 configurations which have survived.

The sensibility of the long–time limit $\langle D \rangle$ to the initial conditions $D(0)$, for fixed temperatures, can be appreciated in Fig. 3. In the intermediate phase (illustrated for $T = 1.04$) $\langle D \rangle$ is independent of the initial non-null $D(0)$, while the opposite happens in the low-temperature regime (illustrated for $T = 0.8$) where $< D >$ is infinitesimally small

for an infinitesimal $D(0)$ and increases almost to 1 as $D(0)$ becomes 1. Taking also into account that $P(t) = 1$ in the intermediate phase, we can thus say that this regime is *fully chaotic* in the sense that even two configurations infinitesimally close at $t = 0$ will always become separated by a *finite* distance.

The three temperature regimes can be also seen in the plot of $< D(t) >$ as a function of T, for different initial conditions, exhibited in Fig. 4. We observe the following: (i) for $T < T_2, < D(t) >$ is non-zero and depends upon the initial $D(0)$; (ii) for $T_2 \leq T < T_1, < D(t) >$ is non-zero and is independent of the initial $D(0)$ and (iii) for $T \geq T_1$, $< D(t) >= 0$ for any initial $D(0)$. This plot corresponds to simulations performed for $L = 64$, $M = 100$ samples and $t = 10000$. The same figure is obtained for $500 \leq t < 10000$ except in the neighborhoods of T_1 and T_2, indicating that outside these small temperature ranges $< D(t) >$ seems to have already reached its long-time limit $< D >$. Concerning the system size dependence, $< D >$ does not vary much with L, the most accentuated differences occuring near the temperature transitions T_1 and T_2. The obtained three-phase diagram is similar to those found in the $3D$ spin glasses [2] and $2D$ XY ferromagnet [6].

The low-temperature regime (i) is consistent with the known phase space structure of the ferromagnetic phase (three distinct valleys with the same energy but different magnetizations): two initial configurations far enough from each other in phase space (such that they are in different valleys at $t = 0$) will remain confined there and keep a finite distance for a long time. This distance presents memory effects (i.e. it remembers for a very long time the initial distance) and it increases monotonously with an increasing $D(0)$. The high-temperature regime (iii) can be also easily understood in terms of the phase space of the paramagnetic phase (one single valley): two configurations will always meet since they are in the same valley and, hence, the damage vanishes. But it is not clear what is the phase space structure corresponding to the intermediate temperature regime (ii) where two distinct initial configurations keep a distance for a very long time (since $P(t) = 1$) and always achieve the same long-time distance for a fixed temperature, no matter how close they are at $t = 0$. Maybe this unusual behavior could be due to a very flat phase space where any two configurations would evolve like two random walks in the phase space which, because of the high dimension, do not meet at reasonable times.

Since the finite time and size effects are more serious near the transition temperatures T_1 and T_2, we follow the finite size scaling procedure [4,6,17] in order to get more reliable estimates for these transition temperatures. For this, we compute first the following quantities for each sample $s(s = 1, 2, \cdots, M)$ of linear size L at the temperature T:

$$\tau_1\ (L, T, s) = \frac{\sum_t t D_s(t)}{\sum_t D_s(t)} \tag{10}$$

$$\tau_2\ (L, T, s) = \frac{\sum_t t^2 D_s(t)}{\sum_t D_s(t)} \tag{11}$$

and the ratio

$$R(L, T, s) = \frac{\tau_2(L, T, s)}{\tau_1^2(L, T, s)} \tag{12}$$

where the samples were iterated until D_s has vanished. τ_1 and τ_2 are measures of characteristic times for two configurations to meet, and both depend upon the size L, the temperature T and the sample s.

One expects the following finite size scaling forms for large L in the neighborhood of the transition temperature T_1:

$$\tau_1(L, T, s) \approx u(L) f_1(v(L)(T - T_1), s) \tag{13}$$

and

$$\tau_2(L, T, s) \approx u^2(L) f_2(v(L)(T - T_1), s) \tag{14}$$

and consequently

$$R(L, T, s) \approx f_3(v(L)(T - T_1, s), \tag{15}$$

where $u(L)$ gives the size dependence at $T = T_1$ (usually $u(L)$ and $v(L)$ are power laws). Taking the average over M samples of Eq. (15) one finally gets that:

$$< R(L, T) > \approx g(v(L)(T - T_1)) \tag{16}$$

from which we conclude that $< R(L, T) >$ becomes independent of L at $T = T_1$. Therefore if we use sufficiently large sizes L_1, L_2, L_3,$\cdots$ their corresponding curves of $< R >$ versus T should cross at the same temperature T_1. In Fig. 5 we show the plots of curves

$< R(L,T) >$, where we have used $L = 16, 32$ and 64 and the set (a) of initial conditions. From this we estimate that

$$\frac{k_B T_1}{J} = 1.13 \pm 0.01 \tag{17}$$

Other initial conditions would give different curves, but crossing at the same temperature given by (17). Notice that this value is unexpectedly close to the exact static critical temperature $k_B T_c \ (q = 2)/J = [\ell n(1 + \sqrt{2})]^{-1} = 1.13459\cdots$ of the square lattice Ising ferromagnet.

In order to determine the other transition temperature T_2 we follow the same procedure used for the XY model in Ref. [6]. Consider, thus, three different replicas A, B and C and define the following measure $\Delta(t)$ for comparing the evolution of $\{\sigma_i^A(t)\}$, $\{\sigma_i^B(t)\}$ and $\{\sigma_i^C(t)\}$ starting from chosen initial configurations $\{\sigma_i^A(0)\}$, $\{\sigma_i^B(0)\}$ and $\{\sigma_i^C(0)\}$:

$$\Delta(t) = D_{AC}(t) - D_{AB}(t) \tag{18}$$

The temperature dependence of the average $< \Delta(t) >$ using the set of initial conditions (d) is shown in Fig. 6. We see from it that $< \Delta(t) >$ for a sufficiently long time t plays the role of order parameter for the continuous transition at T_2 similar to the role of $< D >$ for the transition at T_1. We can thus characterize the three dynamical phases in terms of the two order parameters $< D >$ and $< \Delta >$ as: (i) for $T < T_2$, $< D > \neq 0$ and $< \Delta > \neq 0$; (ii) for $T_2 \leq T < T_1$, $< D > \neq 0$ and $< \Delta > = 0$; (iii) for $T \geq T_1$, $< D > = < \Delta > = 0$.

Defining $\tau_1^{(\Delta)}(L,T,s)$, $\tau_2^{(\Delta)}(L,T)$ and $R^{(\Delta)}(L,T,s)$ in a similar way to the respective Eqs. (10), (11) and (12), with $D_s(t)$ being replaced by $\Delta_s(t)$ (and performing the sum until $\Delta_s(t)$ vanishes for the first time) we obtain the temperature dependence of the average $< R^{(\Delta)} >$ drawn in Fig. 7. These curves cross at the temperature

$$\frac{k_B T_2}{J} = 0.99 \pm 0.01 \tag{19}$$

Notice that this estimate for the temperature transition T_2 below which $< D >$ depends on the initial damage is very close to the exact critical temperature $0.99497\cdots$ of the 3-state Potts ferromagnet at thermal equilibrium. A similar fact has been observed for the $3D$ spin glasses [2] and the $2D$ XY model [6].

B. DYNAMICAL CRITICAL EXPONENTS

Similar to Wang et al [17], we compute the relaxation time critical exponents $z_1 \equiv z(T_1)$ and $z_2 \equiv z(T_2)$ (defined as $\tau \sim \xi^z$, where τ and ξ are temporal and spatial correlation lengths) through the respective average time $\tau_1(L,T_1)$ and $\tau_1^{(\Delta)}(L,T_2)$ for $< D >$ and $< \Delta >$ to vanish, in other words, we suppose that

$$\tau_1\ (L,T_1) \equiv \frac{\sum_t\ t < D(t) >}{\sum_t < D(t) >} \sim L^{z_1} \tag{20}$$

and similarly for $\tau_1^{(\Delta)}(L,T_2)$ replacing $< D(t) >$ by $< \Delta(t) >$.

In Figs. 8(a) and (b) we present the respective log-log plots of τ_1 and $\tau_1^{(\Delta)}$ versus L, where the simulations were performed at the *exact* static critical temperatures T_c $(q = 2)$ and T_c $(q = 3)$ which we believe to be the exact values for T_1 and T_2. From the slope of the lines we estimate that

$$z_1 = 1.54 \pm 0.02 \tag{21}$$

and

$$z_2 = 2.28 \pm 0.03 \tag{22}$$

Notice that z_2 compares well with the recent accurate value $z \simeq 2.196$ computed for the 3-state Potts model from short-time dynamics [31] and with other previous results where $2.1 \leq z \leq 2.8$ (see [32] and references therein, [33]). In contrast, z_1 is far from the recent accurate value 2.172 ± 0.006 [19] and from other results $(1.9 < z < 2.3)$ quoted in the literature for the $2D$ Ising ferromagnet [32,14,17,20,21]. This indicates that the dynamic transition at T_1, although is consistent with the static Ising critical temperature, is not in the Ising universality class since the damage spreading technique within the heat bath dynamics has led, for the Ising model, estimates for z [14,17,19–21] which agree with those derived from other methods. Notice that a similar discrepancy in the universality class also happens in the upper transition of spin glasses, where T_1 corresponds to the critical point of the bond frustrated percolation and the critical exponents are in the standard bond percolation universality class [10,34].

In Fig. 9 we present the temporal behavior of $\langle D(t)\rangle$ for $L = 256$ at different temperatures in the range $1.129 \leq T \leq 1.137$. In the case of $T = T_c(q = 2)$ we have also obtained $\langle D(t, L = 128)\rangle$ (not shown herein) which, for $60 < t < 200$, becomes identical to $\langle D(t, L = 256)\rangle$ and has a power law decay ($\langle D(t)\rangle \sim t^{-\delta}$) [4,17–19]. In general $\langle D(t, L)\rangle$ is expected to follow [4], at $T = T_c$ and $t >> 1$ and $L >> 1$, the finite size scaling form $\langle D(t, L)\rangle \sim L^{-\delta z} f(t/L^z)$ where $f(x) \sim x^{-\delta}$ (for $x << 1$) leading thus, for $t << L^z$, to the above mentioned time decay. Therefore the time range $60 < t < 200$ over which our results for $\langle D(t, L)\rangle$ become size independent corresponds to the validity region of the power law decay $t^{-\delta}$. Taking this into account, we can extract from Fig. 9 an estimate for T_1 which has a better accuracy than that of Eq. 17, namely:

$$\frac{k_B T_1}{J} = 1.135 \pm 0.003 \tag{23}$$

From the slope of $\langle D(t)\rangle$ at $T = T_1$ in this time region we obtain that

$$\delta = 0.46 \pm 0.03 \tag{24}$$

which is compatible with the value $\delta \simeq 0.46$ for the directed percolation (DP) in $2 + 1$ dimensions [18]. A similar value was obtained in [18] where the spreading transition temperature disagrees with the static critical temperature. Our result (as well as that of [18]) corroborates Grassberger's conjecture [35] since the transition at T_1 does not coincide with the static 3-state Potts one.

We have also examined the time evolution of $< \Delta(t) >$ at temperatures around T_2. Our curves (not shown herein) present also a power law decay at $T = T_c$ ($q = 3$), but our statistics (2000 samples of size $L = 256$) was not sufficient for computing a reliable estimate of δ since in this case the survival probability of Δ is considerably smaller than 1 and the relaxation time is much bigger ($\tau_1^{(\Delta)} \simeq 60\ \tau_1$ for $L = 256$).

IV. INFLUENCE OF EXTERNAL FIELDS

In Fig. 10 we show the graphic of the long–time $< D >$ as a function of temperature T when a magnetic field of strength $B = 0.01$ (see Eq. 1)) is applied. The simulations were performed for the sets of initial conditions *(a)* (represented by squares) and *(b)*

(represented by circles). For comparison, we also include points (represented by triangles) corresponding to a zero-field and set *(a)* of initial configurations. From this we see that both transitions persist under the application of a magnetic field, similarly to the $2D$ [18] and $3D$ [7,18] Ising ferromagnets with Glauber dynamics. Consequently *the magnetic field is neither the conjugate field associated with the order parameter* $< D >$ *nor that associated with* $< \Delta >$.

A new kind of external field h has been introduced a few years ago [28], in the context of the Domany-Kinzel cellular automaton (see ref. [36]), which destroys the damage transition and leads to the divergence of its associated susceptibility.

$$\chi_h \equiv \frac{\partial < D >}{\partial h}|_{h \to 0} \tag{25}$$

at the transition. They defined h *as the frequency at which distinct random numbers are used to update the two replicas*, weakening thus the coupling between the replicas. A mean-field analysis [29] of this cellular automaton predicted the same type of behavior for χ_h. More recently numerical simulations of the damage spreading on the $2D$ Ising ferromagnet [15] also showed that h plays the role of a conjugate field to the Hamming distance $< D(t) >$.

The results of the application of such an external field h (for $h = 0.005$ and $h = 0.010$) are exhibited in Fig. 11; it is also shown, for comparison, $< D(t) >$ for $h = 0$. One clearly sees that a small h destroys the continuous damage spreading transition observed for $h = 0$ at $T = T_1$. Since there is no analog to the fluctuation-dissipation theorem for the damage, we obtain an approximation for the zero-field susceptibility χ_h by calculating the variation of the damage $< D(t) >$ corresponding to a small change of h. Fig. 12 displays these approximations for χ_h versus T for the above values of the field. We observe, similarly to the $2D$ Ising ferromagnet [15], a tendency for χ_h to diverge near the corresponding transition temperature T_1 as $h \to 0$, indicating thus that h is the conjugate field $< D >$. Concerning the other transition at T_2, the situation is more complicate since it involves the comparison of three replicas, and we have not succeeded in finding out a conjugate field to $< \Delta >$.

V. CONCLUSIONS

The dynamical behavior of the 3-state Potts ferromagnet on the square lattice is investigated through the damage spreading method within the heat bath dynamics. We found that this is the simplest spin model studied so far which presents a three-phase structure similar to that encountered in more complex systems, like the $3D$ spin glasses [2,10] and $2D$ XY ferromagnet [5]. Furthermore, the unexpected chaotic phase which appears above the static Potts critical temperature $T_2 = T_c$ $(q = 3)$ and below the static Ising one $T_1 = T_c$ $(q = 2)$ has unusual features. In this phase, two initial configurations stay different for a very long time (since the survival probability $P(t)$ equals 1) and always achieve, for a fixed temperature, the same long-time Hamming distance no matter how close they are at $t = 0$. Maybe this is due, in terms of energy landscape, to an extensive flattening where any two configurations would evolve like two random walks which do not cross at reasonable times because of the high dimensionality of the phase space. Another odd result concerning the new phase was obtained, namely: despite its upper boundary T_1 occurs, within the error bars, at T_c $(q = 2)$, its corresponding dynamic critical exponent z_1 differs a lot from the reported values for the Ising model. The short-time decay exponent δ of the Hamming distance indicates that this transition is in the $(2 + 1)$-dimensional directed percolation universality class, in agreement with Grassberger's conjecture [35]. We have also verified that the new kind of external field h introduced a few years ago [28] plays the role of a conjugate field to the order parameter $< D >$ of this transition, i.e., it destroys the transition at T_1 observed at $h = 0$ and its associated susceptibility diverges at T_1.

It would be interesting to investigate the long-time behavior of the spin autocorrelation function $C(t)$ in each of the three dynamical phases in order to see, in particular, how its functional form in the low-temperature regime differs from that of the intermediate one. Since we found that the relaxation time at T_1 is smaller than at T_2 (as $z_1 < z_2$) and that the memory effect of the initial damage disappears for $T \geq T_2$, we expect that (similarly to the $3D$ spin glasses [23,24]) $C(t)$ in the intermediate phase decays slower than in the high temperature regime (where it is probably given by a simple exponential decay) but faster than in the low-temperature one (where it could be

eventually given by a stretched exponential decay similar to that found for the $2D$ Ising ferromagnet [37,22]). Work along this line is in progress.

Further studies are needed to clarify the real nature of the unexpected phase. In particular, it remains to check if its upper boundary T_1 is exactly equal to T_c ($q = 2$) and, in the affirmative case, it would be very interesting to understand the profound reasons for this coincidence.

Acknowledgements: We acknowledge C. Tsallis and E.M.F. Curado for fruitful discussions. We thank CNPq and VITAE Foundation for financial support. Part of the simulations were carried out on a CRAY J90 of NACAD-COPPE/UFRJ.

FIGURES

FIG. 1. The survival probability $P(t)$ versus temperature for different values of time. The data for $t = 9000$ and 10000 coincide within the used scale. $M = 100$ samples of linear size $L = 64$ with initial configurations *(c)* (where $D(0) = 0.05$) were examined.

FIG. 2. Time evolutions of $< D(t) > (- \cdot\cdot -), < d(t) > (\cdots)$ and the survival probability $P(t)(-\cdot -)$ for the fixed temperatures $k_BT/J = 0.90$ (a) and $k_BT/J = 1.06$ (b). The simulations were performed on $M = 100$ samples of linear size $L = 64$ with the set of initial conditions *(b)* ($D(0) = 1/2$). We also represent in Fig. 2a, by a full line, the results for an initial damage $D(0) = 1$ (initial configurations *(a)*) where $< D(t) >=< d(t) >$ since $P(t) = 1$ in this case.

FIG. 3. Plot of $< D(t = 10000) >$ versus the initial damage $D(0)$ for the fixed temperatures $k_BT/J = 0.80$ (represented by black dots) and $k_BT/J = 1.04$ (represented by white dots). The results for $t = 1000$ are also shown (by squares) when $T = 1.04$. We performed the averages over $M = 20$ samples of size $L = 64$ at $k_BT/J = 1.04$, while the number of replicas varied from 50 to 1000 at the other temperature. The inset shows the results for $k_BT/J = 0.80$ in the region near $D(0) = 0$.

FIG. 4. Average damage $< D >$ versus temperature for three different initial damages *(a)* $D(0) = 1$, *(b)* $D(0) = 0.5$ and *(c)* $D(0) = 0.05$. Simulations were performed for $M = 100$ samples of linear size $L = 64$ and $t = 10000$.

FIG. 5. The ratio $< R >=< \tau_2/\tau_1^2 >$ versus temperature for distinct sizes L. The number M of used samples were at most 16000, 10000 and 500 for $L = 16, 32$ and 64, respectively. The initial damage was $D(0) = 1$ (set *(a)* of initial configurations). The error bars are smaller than the symbols. The arrow signals the exact static Ising critical temperature.

FIG. 6. $< \Delta >$ as a function of temperature. The simulations were performed at $t = 2000$ for $M = 200$ samples of size $L = 64$ with initial conditions *(d)*.

FIG. 7. The ratio $< R^{(\Delta)} >=< \tau_2^{(\Delta)}/(\tau_1^{(\Delta)})^2 >$ versus temperature for different sizes. We used at most $M = 10000$, 1000 and 250 replicas for the respective sizes $L = 16, 32$ and 64 with initial configurations *(d)*. The error bars are smaller than the symbols. The arrow signals the exact static critical temperature T_c $(q = 3)$.

FIG. 8. Log-log plots of the vanishing times τ_1 (a) and $\tau_1^{(\Delta)}$ (b) against the linear lattice size L calculated at the temperatures T_c $(q = 2)$ and T_c $(q = 3)$, respectively. In (a) we averaged over 16000, 10000, 4000 and 500 samples of respective linear sizes $L = 8, 16, 32$ and 64 with initial damage $D(0) = 1/2$ (set of configurations *(b)*). In (b) we used $M = 40000, 20000, 20000$ and 7000 of respective sizes $L = 8, 16, 32$ and 64 with the set of initial conditions *(d)*. The straight lines correspond to $z = 1.54$ (Fig. 8a) and $z = 2.28$ (Fig. 8b).

FIG. 9. Log-log plot of $< D >$ versus time t at the following fixed temperatures k_BT/J from top to bottom: 1.131, 1.1325, $k_BT_c(q = 2)/J$ and 1.137. The results were averaged over 100 samples of linear size $L = 256$ with initial damage $D(0) = 1$ (configurations $\{\sigma_i^A(0)\}$ is random and configuration $\{\sigma_i^B(0)\} \neq \{\sigma_i^A(0)\} \forall i$). The dotted line (whose intercept is arbitrary) has the slope -0.46 predicted from the directed percolation.

FIG. 10. The average damage $< D\ (t = 10000) >$ as a function of temperature for a magnetic field strength $B = 0.01$ and sets of initial configurations *(a)* (open squares) and *(b)* (open circles). For comparison, we also represent (by full triangles) the results in a zero magnetic field with initial damage $D(0) = 1$. We used 200 samples of size $L = 64$.

FIG. 11. The temperature dependence of $< D\ (t = 4100) >$ for different values of the external field h. We used $M = 100$ samples of linear size $L = 64$ with set *(b)* of initial configurations.

FIG. 12. Approximations for the susceptibility χ_h (defined in Eq. (5)) versus temperature obtained from the results of Fig. 11. The arrow signals the exact static Ising critical temperature T_c $(q = 2)$.

REFERENCES

[1] Costa U M S 1987 *J. Phys. A* **20** L583.

[2] Derrida B and Weisbuch G 1987 *Europhys. Lett.* **4** 657.

[3] Barber M N and Derrida B 1988 *J. Stat. Phys.* **51** 877.

[4] Newmann A U and Derrida B 1988 *J. Phys. France* **49** 1647.

[5] Golinelli O and Derrida B 1988 *J. Phys. France* **49** 1663.

[6] Golinelli O and Derrida B 1989 *J. Phys. A* **22** L939.

[7] Le Caer G 1989 *J. Phys. A* **22** L647 and *Physica* **A159**, 329 (1989).

[8] Chiu J and Teitel S 1990 *J. Phys. A* **23** L891.

[9] Mariz A M 1990 *J. Phys. A* **23** 979.

[10] De Arcangelis L 1990, in *Correlations and Connectivity*, edited by Stanley H E and Ostrowsky N (Kluver Acad. Publ.).

[11] Golinelli O 1990 *Physica A* **167** 736.

[12] Leroyer Y and Rouidi K 1991 *J. Phys. A* **24** 1931.

[13] Miranda E N and Parga N 1991 *J. Phys.* **A24** 1059.

[14] Stauffer D 1993 *J. Phys. A* **26** L599.

[15] Tamarit F A and da Silva L 1994 *J. Phys. A* **27** L809.

[16] Tamarit F A and Curado E M F 1994 *J. Phys. A* **27** 671.

[17] Wang F, Hatano N and Suzuki M 1995 *J. Phys. A* **28** 4543.

[18] Grassberger P 1995 *J. Phys. A* **28** L67.

[19] Grassberger P 1995 *Physica A* **214** 547 and **217** 227 (erratum).

[20] Gropengiesser U 1995 *Physica A* **215** 308.

[21] Wang F and Suzuki M 1996 *Physica A* **223** 34.

[22] Grassberger P and Stauffer D, to be published.

[23] Ogielski A T 1985 *Phys. Rev. B* **32** 7384.

[24] Campbell I A 1986 *Phys. Rev. B* **33** 3587.

[25] Wu F Y 1982 *Rev. Mod. Phys.* **54** 235; Tsallis C and de Magalhães A C N 1996 *Phys. Rep.* **268** 305.

[26] Bibiano M F A, Moreira F B and Mariz A M, private communication.

[27] Palandi J, de Almeida R M C and Iglesias J R, private communication.

[28] Tsallis C and Martins M L 1994 *Europhys. Lett.* **27** 415.

[29] Tomé T 1994 *Physica A* **212** 99.

[30] da Silva L, Tamarit F A and de Magalhães A C N, to be published.

[31] Schülke L and Zheng B 1995 *Phys. Lett. A* **204** 295.

[32] Tang S and Landau D P 1987 *Phys. Rev. B* **36** 567.

[33] Aydin M and Yalabik M C 1988 *J. Phys. A* **21** 769, 1984 **17** 2531 and 1985 **18** 1741.

[34] De Arcangelis L, Coniglio A and Peruggi F 1991 *Europhys. Lett.* **14** 515.

[35] Grassberger P 1995 *J. Stat. Phys.* **79** 13.

[36] Martins M L, de Resende H F V, Tsallis C and de Magalhães A C N 1991 *Phys. Rev. Lett.* **66** 2045.

[37] Huse D A and Fisher D S 1987 *Phys. Rev.* **B35** 6841.

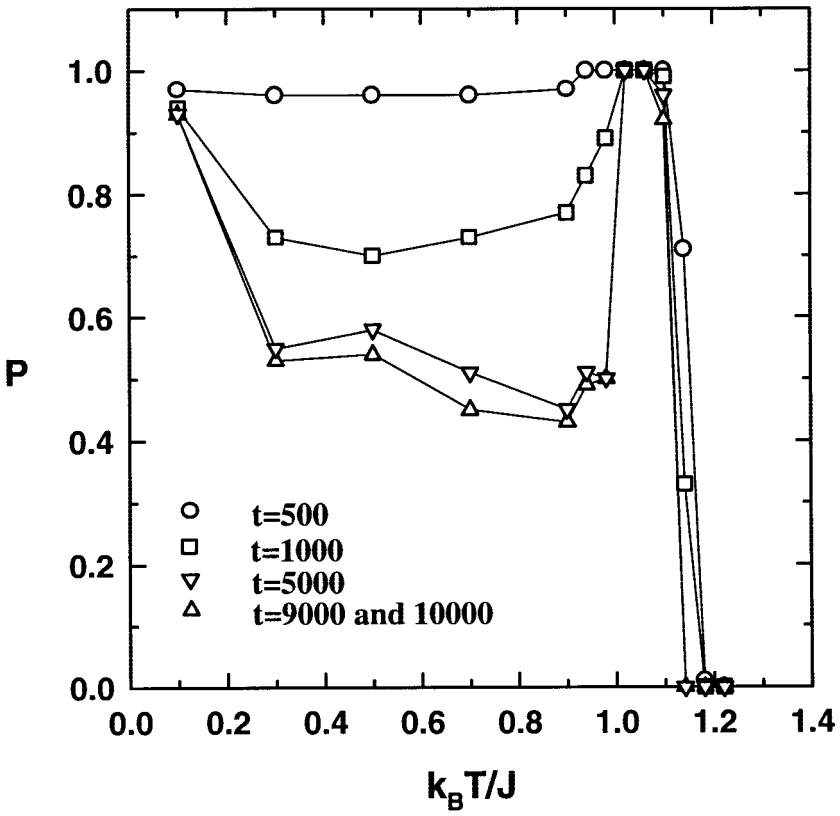
P
1.0
0.8
0.6
0.4
0.2
0.0
0.0
0.2
0.4
0.6
0.8
1.0
1.2
1.4
$k_B T/J$
t=500
t=1000
t=5000
t=9000 and 10000

Fig. 1

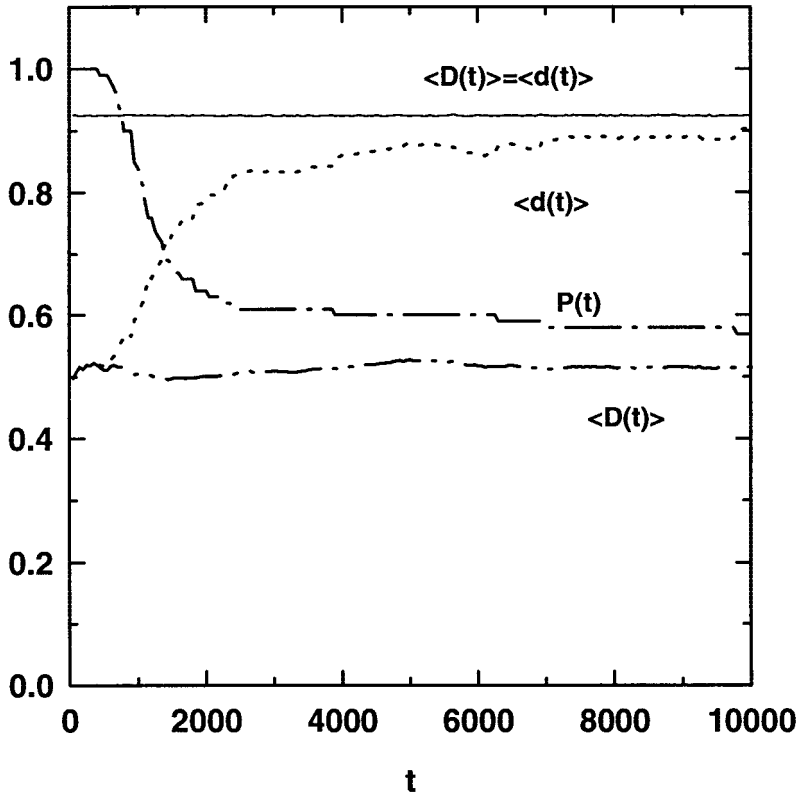

Fig. 2a

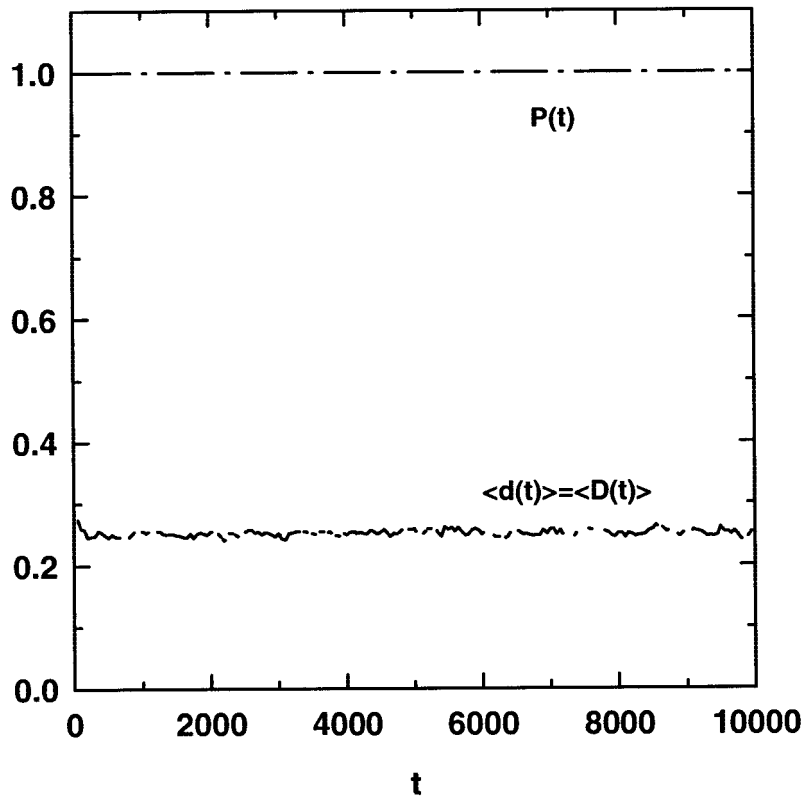

Fig. 2b

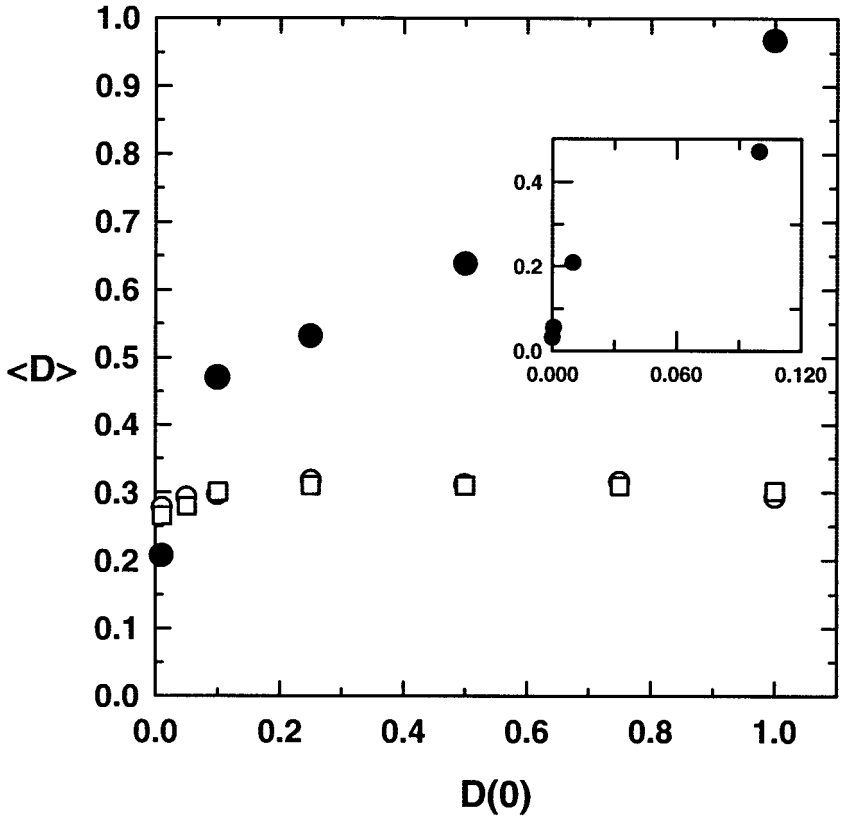

Fig . 3

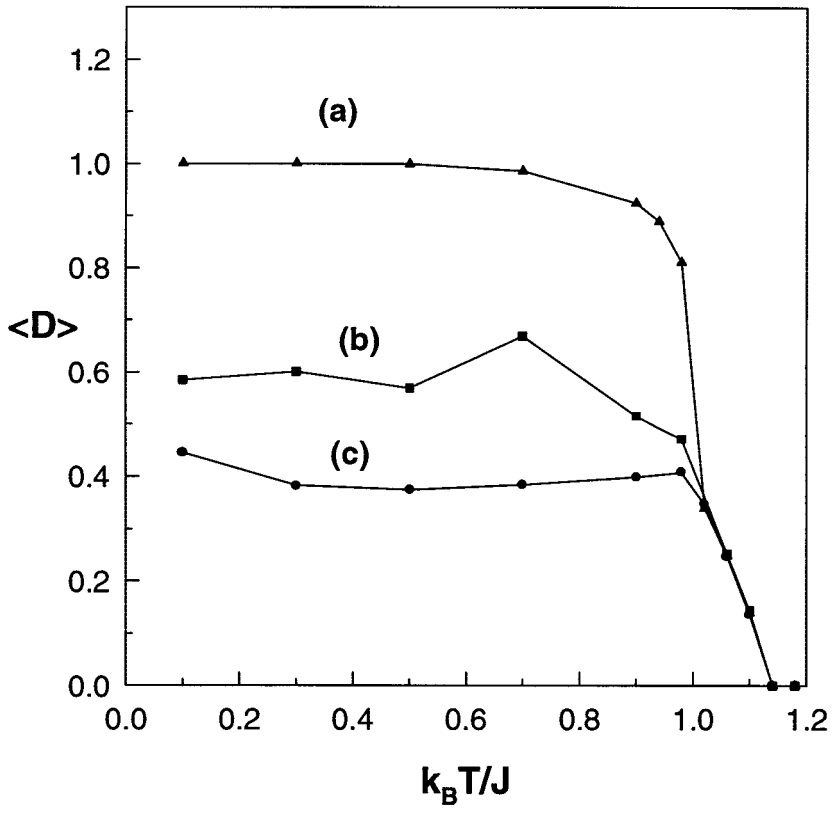

Fig. 4

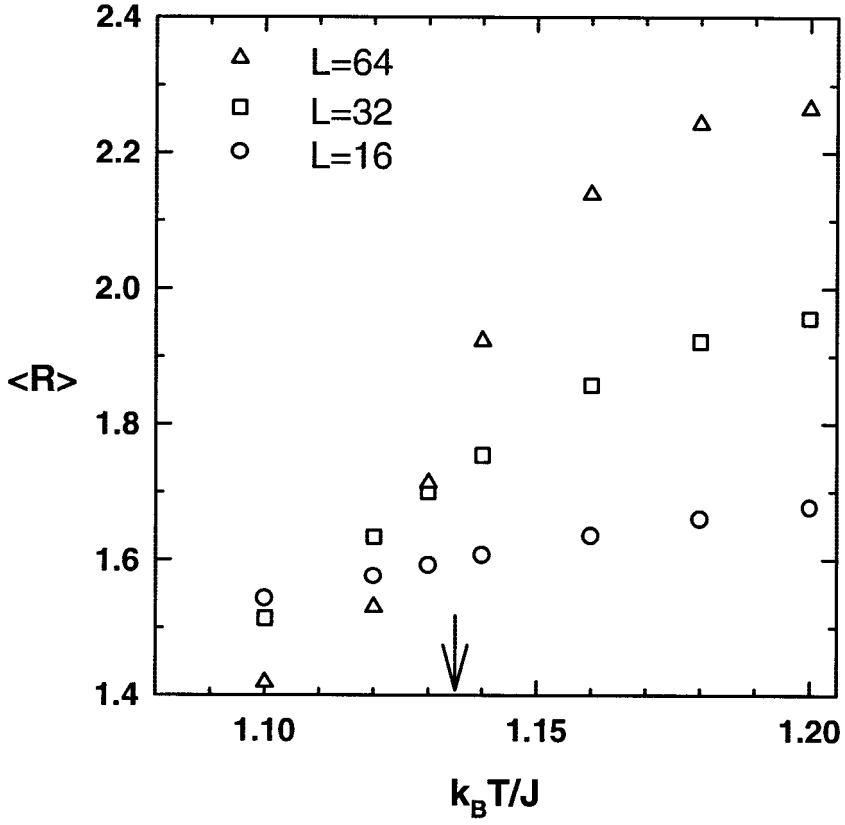

Fig. 5

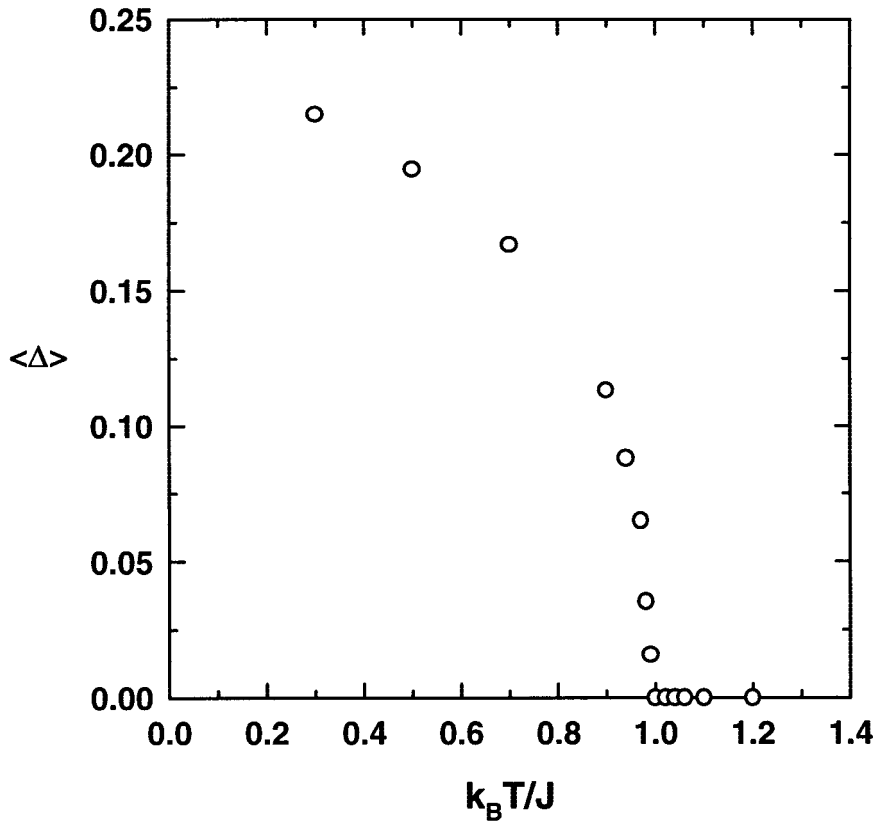

Fig. 6

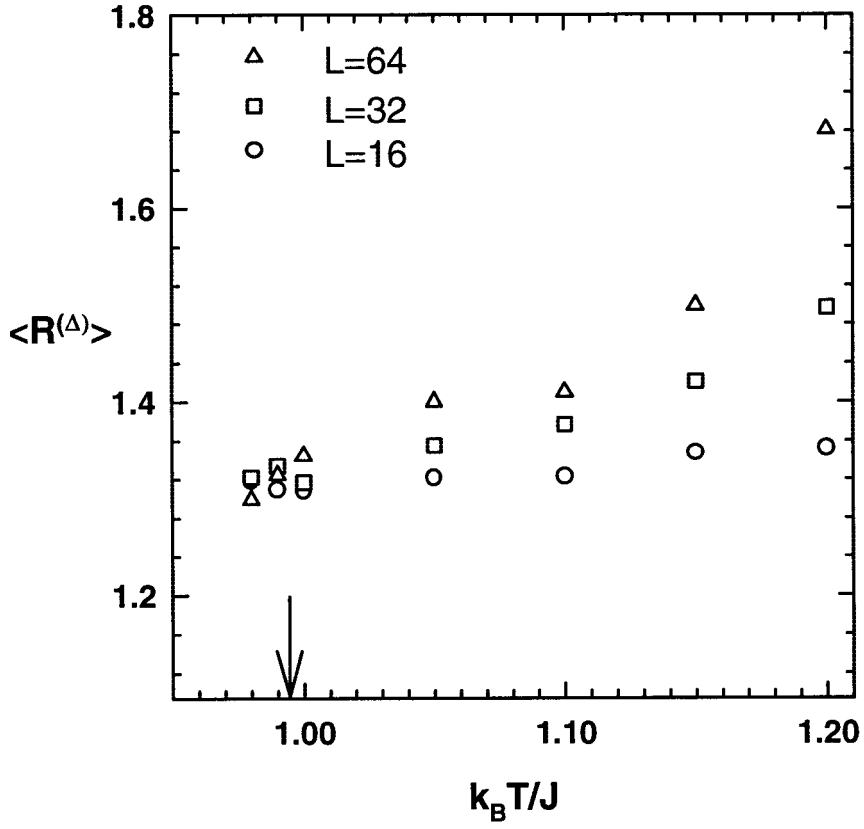

Fig. 7

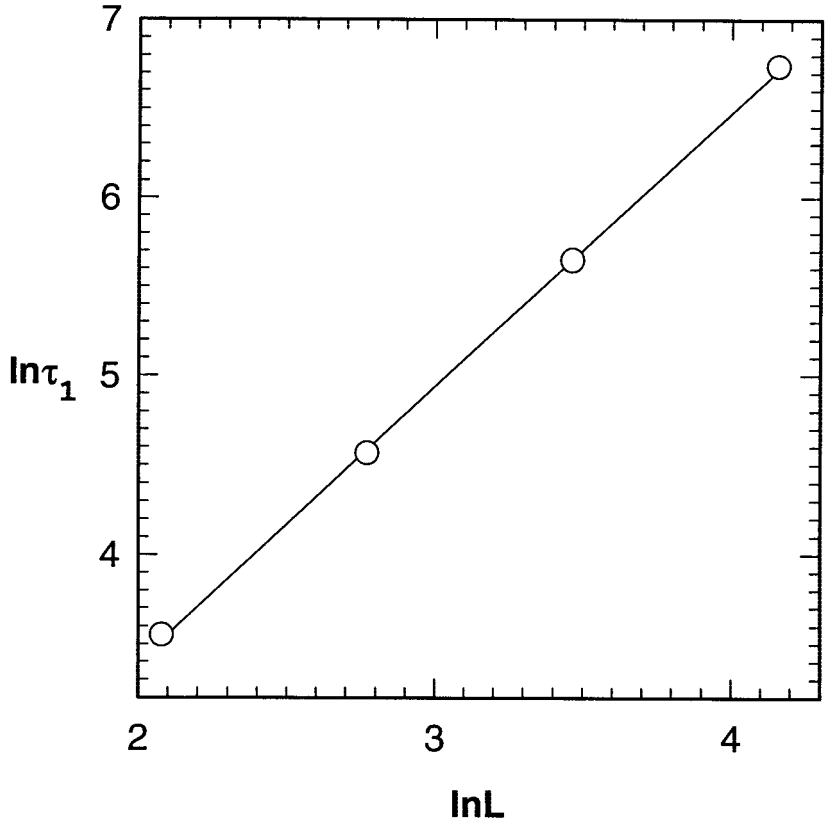

Fig. 8a

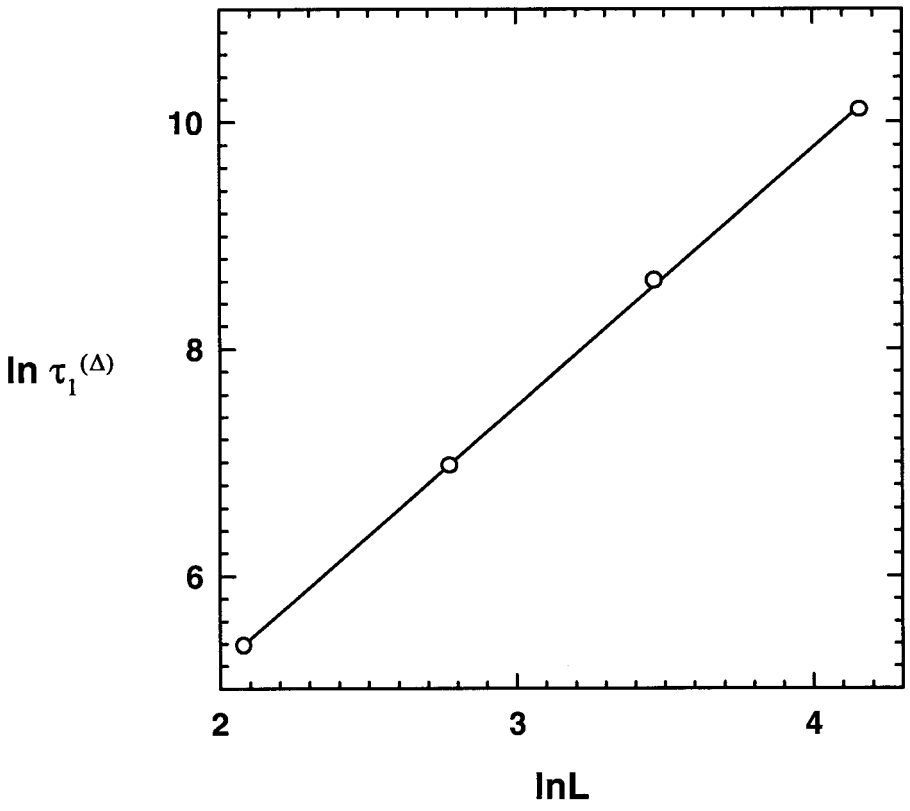

Fig. 8b

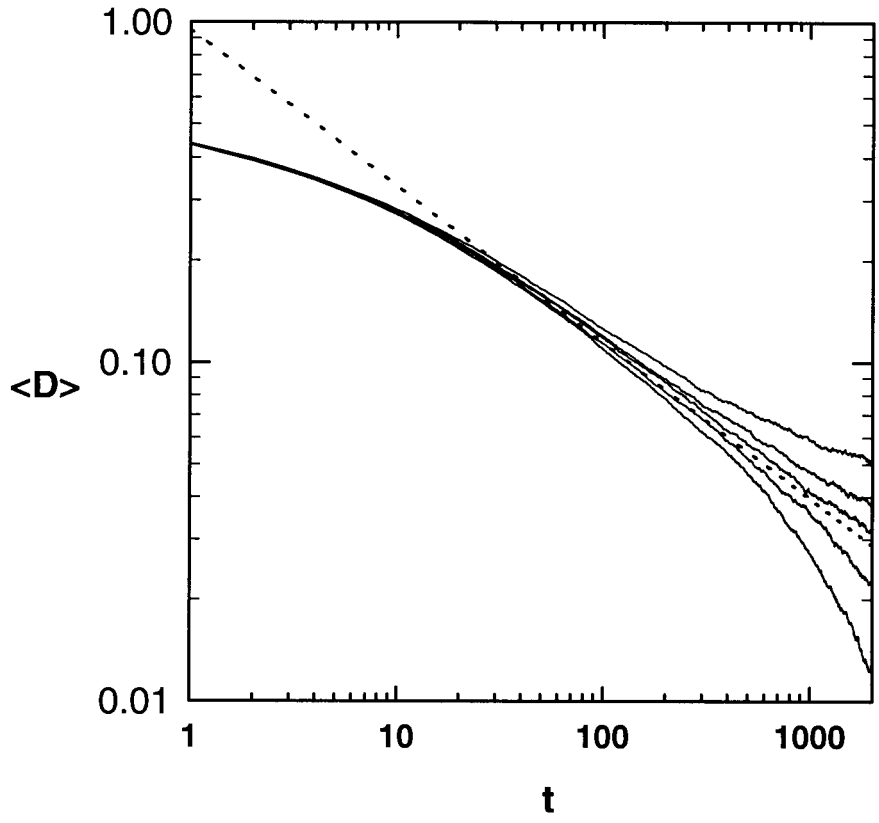

Fig. 9

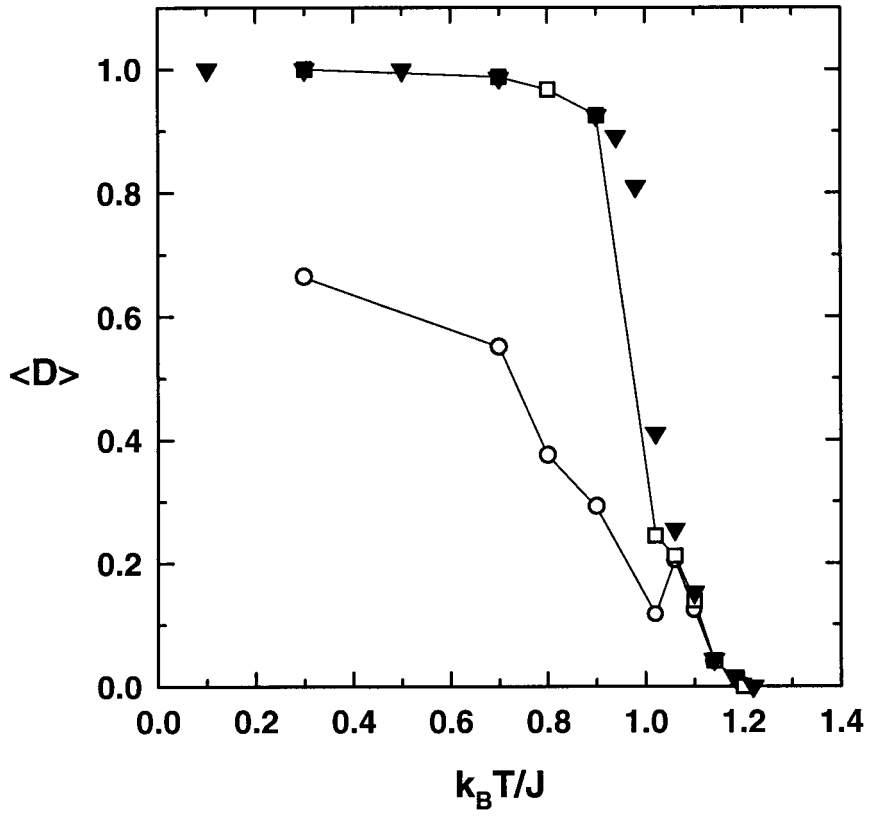

Fig. 10

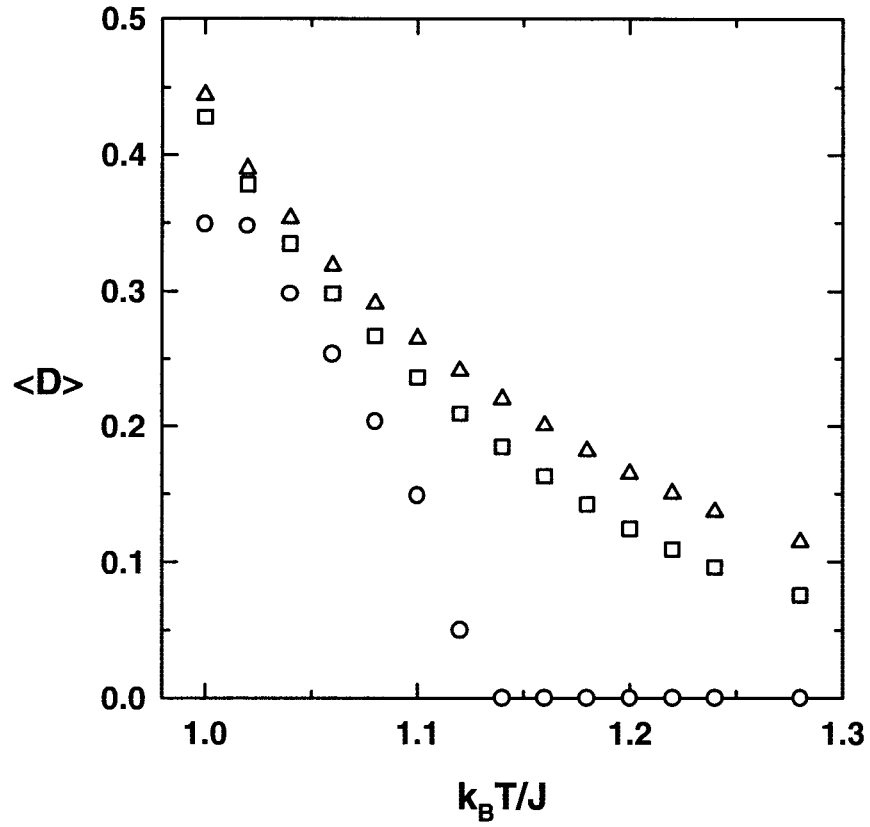

Fig. 11

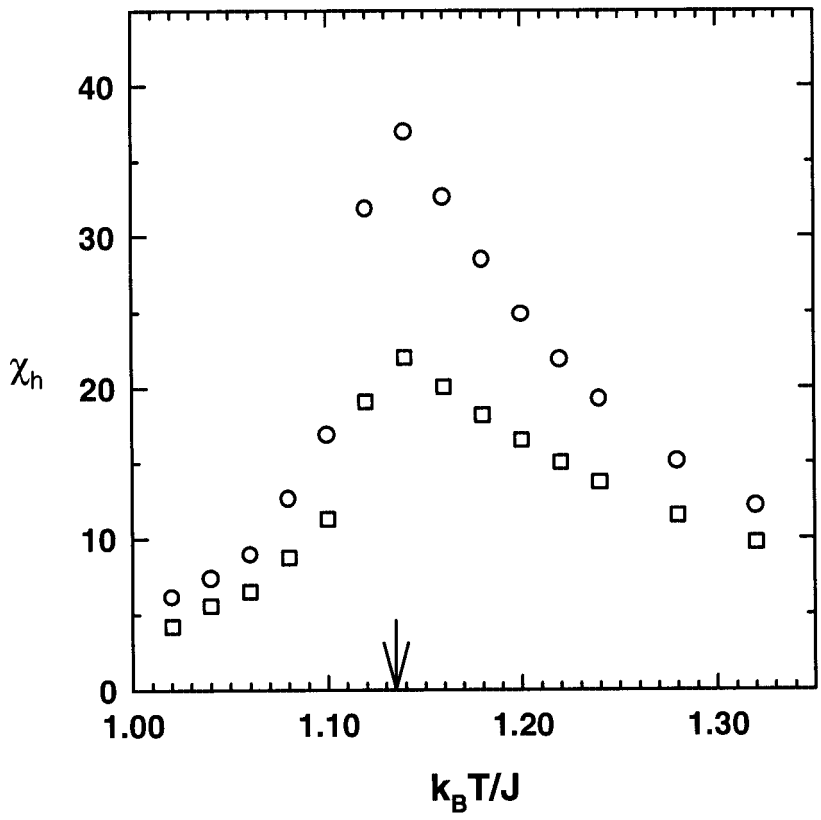

Fig. 12